The influence of oscillatory and steady shears on interfacial stability during directional solidification

T.P. Schulze, S.H. Davis *

Department of Engineering Sciences and Applied Mathematics, Northwestern University, Evanston, Illinois 60208, USA

Abstract

A linear stability analysis is performed on the interface formed during the directional solidification of a dilute binary alloy in the presence of a weak, time-dependent flow. In one case, the flow is generated by a simple harmonic, lateral oscillation of the crystal, resulting in solidification into a compressed Stokes boundary layer. In a second, more general, case, the crystal also has a mean horizontal velocity. The presence of the flow can either stabilize or destabilize the two-dimensional system relative to the case with no flow, with the result depending on the Schmidt number, segregation coefficient, and the frequency of the oscillations.

1. Introduction

The microstructures of solids are determined during their formation, and are, in part, a result of instabilities at the solid–liquid interface. Metallurgists and crystal growers realize that unsteady convection in the melt has a significant effect on this interfacial morphology. Natural convection in the melt can be generated by buoyancy, expansion or contraction upon phase-change, and thermo-soluto capillary effects, the last two playing significant roles in microgravity environments. These flows are strongly nonparallel in nature, frequently exhibiting three-dimensional and time-dependent structures. Flow can also be generated by external forcing, such as rotation of the crystal during the solidification process. There has been much speculation that such flows could be used to gain better control over interfacial morphology, selecting patterns and length scales, and possibly stabilizing an otherwise unstable interface.

The focus here will be on directional solidification, which provides a simple configuration for the study of morphological instability. This arrangement consists of unidirectional solidification in which a binary alloy is pulled across a fixed temperature gradient at constant speed (Fig. 1). The solid–liquid interface will establish itself at a fixed position in a laboratory frame of reference.

In the absence of flow, there is a steady basic state that features a planar interface and an exponentially decaying concentration profile in the melt. The concentration profile has a discontinuity at the interface due to solute rejection. The potential for morphological instability exists as a result of the adverse concentration gradient
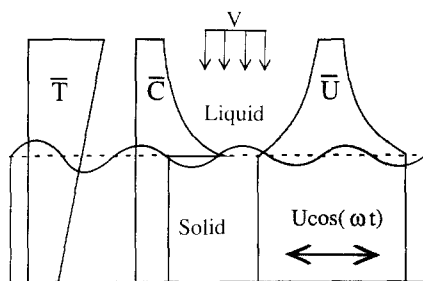
---

* Corresponding author.

Fig. 1. Unidirectional solidification setup shown with basic state temperature, concentration, and velocity profiles.

which raises the melting temperature of the so-lute-laden material near the interface. The morphological instability of the solid–liquid interface is primarily governed by three parameters: the average concentration of solute C_∞, the pulling speed V, and the overall temperature gradient G. Mullins and Sekerka [14] performed a linear stability analysis on this system, and found that the interface undergoes a cellular instability for a certain range of the parameters, resulting in a steady corrugated interface.

Numerous studies have been done investigating the effect of flow during directional solidification. As with most fluid systems, the analysis is considerably simplified by focussing on parallel-flow situations. Delves [7] studied solidification into a Blasius boundary layer, using a parallel-flow approximation. Coriell, McFadden, Boisvert and Sekerka [2] numerically investigated solidification into a plane Couette flow (linear velocity profile). These studies found that disturbances with wave vectors parallel to the flow are stabilized. Disturbances with wave vectors perpendicular to the flow are left unaffected, a result that will hold for any flow with only one nontrivial velocity component in the plane of the crystal interface.

Forth and Wheeler [8] investigated solidification into a parallel flow with the asymptotic suction profile (ASP). Such a profile would result from translating the crystal horizontally at constant speed during directional solidification. They present linear stability results from asymptotics valid for large Schmidt number. It is clear from their results that the flow can either stabilize or destabilize disturbances parallel to the flow, with

the longer wavelength disturbances tending to grow slower, and the shorter wavelength disturbances tending to grow faster. They pointed out that their asymptotic expansions are not uniformly valid in the limit of long waves or large Reynolds numbers. They also presented results of a numerical study that indicates that shorter wavelengths are further stabilized by increasing the Reynolds number.

Hobbs and Metzener [10] also considered how the flow with the ASP affects morphological stability. Their work is primarily concerned with resolving the nonuniformities for long-wave disturbances encountered near the absolute stability boundary. They use singular perturbation techniques to consider the limits of small flow speed, small segregation coefficient, and large Schmidt number.

Merchant and Davis [13] considered the effect of a temporally modulated stagnation-point flow on the morphological stability of a directionally-solidifying interface. They studied the influence of this unsteady, nonparallel flow using a long-wave analysis, and found that low-frequency modulation was always stabilizing, while high-frequency modulation was always destabilizing.

For a more extensive review of research on the role of convection in solidification see Coriell, McFadden and Sekerka [3], Glicksman, Coriell and McFadden [9], Davis [4–6], and Coriell and McFadden [1].

In this paper we study the influence of a Stokes boundary layer on morphological stability. One can imagine this flow being generated by oscillating the crystal in the horizontal plane as the material is solidified upward (Fig. 1). The boundary layer is compressed as a result of flow perpendicular to the interface generated by the pulling velocity. We refer to this flow configuration as a compressed Stokes layer (CSL). The relationship between a Stokes layer and a CSL is analogous to that between plane Couette flow and a flow with the ASP.

As with these previous studies, we neglect all other sources of convection: gravity, changes in density during phase change, and thermo-soluto capillary effects. We also neglect the influence of any horizontal boundaries by assuming the spatial

domain to be infinite. This is justified because the length scale of the instabilities to be studied is much smaller than the width of any realistic container. Like the ASP, the CSL is also a parallel flow, but this time-dependent basic state introduces a new control parameter, the frequency, into the system that may potentially be manipulated to the crystal growers advantage.

To gain further control over the system through the use of a forced flow, one can combine an oscillatory motion of the crystal with a steady translation. We report linear stability results for this general case in the limit of small forcing. We consider the two-dimensional case since disturbances perpendicular to the parallel flow are unaffected.

We begin in the next section by presenting the governing equations and making a few simplifying assumptions. In Section 3, we present the linearized disturbance equations and briefly review the results for the case without flow. In Section 4, we look at the CSL by itself, and in Section 5, we review the ASP results, pointing out some minor differences with the results of Hobbs and Metzener [10]. In Section 6 we explore the combined case, and in Section 7 we offer some explanation of the physical mechanisms involved in this system. Finally, in Section 8 we summarize and conclude.

2. Governing equations

Consider a coordinate system with x-axis located at the mean position of the crystal interface, moving with the front, and a z-axis that is fixed in the laboratory frame of reference. The equations governing the system in the fluid region are the Navier–Stokes, continuity, solute diffusion, and thermal diffusion equations:

$$u_t + u \cdot \nabla u - V u_z = -\frac{1}{\rho} \nabla p + \nu \nabla^2 u, \qquad (2.1a)$$

$$\nabla \cdot u = 0, \qquad (2.1b)$$

$$C_t + u \cdot \nabla C - V C_z = D \nabla^2 C, \qquad (2.1c)$$

$$T_t + u \cdot \nabla T - V T_z = \kappa \nabla^2 T, \qquad (2.1d)$$

where u is the fluid-velocity vector, p is the fluid pressure, C is the concentration of the dilute component of the binary mixture, T is the temperature in the fluid, ρ is the density of the mixture (assumed equal in both the liquid and solid phase), κ is the thermal diffusivity, and D is the solute diffusivity. The subscripts denote differentiation with respect to time (t) and space (x, z). ∇ is the gradient operator, and ∇^2 is the Laplacian. The translational term in these equations is the result of the fluid velocity being measured in the reference frame of the quiescent fluid. This is done so that the vertical velocity at the interface will be zero.

We shall make the frozen-temperature approximation [12]. In this limit we neglect latent heat, assume equal thermal properties in the liquid and solid phases, and assume that the diffusion of heat is much faster than the diffusion of solute. Under these assumptions the temperature field has a fixed linear profile,

$$T = T_0 + Gz, \qquad (2.2)$$

where T_0 is the temperature at the interface in the basic state and G is the temperature gradient.

We shall be investigating what happens when the crystal undergoes lateral motion. To simplify our analysis, we transform to a reference frame where the crystal is stationary, and the fluid in the far field moves instead. This involves the following two changes:

$$u \to u + U[(1 - R) \cos (\omega t) + R], \qquad (2.3a)$$

$$x \to x + U\left[\frac{1 - R}{\omega} \sin (\omega t) + Rt\right], \qquad (2.3b)$$

where $u(x, 0, t) = U[(1 - R) \cos (\omega t) + R]$ is the horizontal velocity of the crystal in the old reference frame. Here, the amplitude of the velocity oscillations added to the magnitude of the steady shear is U, R indicates the fraction of the flow that is steady, and ω is the frequency of the oscillations. When $R = 0$, the flow will be purely oscillatory. When $R = 1$, the flow will be a steady shear. These transformations leave the equations unchanged, except for a time dependent forcing

term in the horizontal component of the Navier–Stokes equations.

We nondimensionalize our equations with the following scalings:

$$x \rightarrow (D/V)x \tag{2.4a}$$

$$u \rightarrow Uu \tag{2.4b}$$

$$t \rightarrow t/\omega \tag{2.4c}$$

$$p \rightarrow \rho UVp \tag{2.4d}$$

$$T \rightarrow (GD/V)T + T_0 \tag{2.4e}$$

$$C \rightarrow (C_\infty - C_\infty/k)C + C_\infty/k, \tag{2.4f}$$

where D is the solute diffusivity, V is the crystal pulling speed, ρ is the material density, C_∞ is the far field concentration, and k is the segregation coefficient.

With these revisions, the governing equations are

$$\Omega u_t + \epsilon u \cdot \nabla u - u_z$$

$$= -\nabla p + S\nabla^2 u + i(1-R)\Omega \sin t, \tag{2.5a}$$

$$\nabla \cdot u = 0, \tag{2.5b}$$

$$\Omega C_t + \epsilon u \cdot \nabla C - C_z = \nabla^2 C, \tag{2.5c}$$

$$T = z, \tag{2.5d}$$

where

$$\Omega = \omega D/V^2 \tag{2.6}$$

is the nondimensional frequency, $S = \nu/D$ is the Schmidt number, and $\epsilon = U/V$ is the velocity ratio.

As $z \rightarrow \infty$, the far-field boundary conditions are

$$u \rightarrow -[(1-R)\cos t + R], \tag{2.7a}$$

$$w \rightarrow 0, \tag{2.7b}$$

$$C \rightarrow 1, \tag{2.7c}$$

and the interfacial conditions are evaluated at the interface $z = h(x, t)$ are

$$u = 0, \tag{2.8a}$$

$$C = M^{-1}h - 2\Gamma H, \tag{2.8b}$$

$$(1 + \Omega h_t)[1 + (k-1)C] = C_z - C_x h_x. \tag{2.8c}$$

Here, the morphological number is

$$M = mVC_\infty(1 - 1/k)/GD, \tag{2.9}$$

where m is the liquidus slope in the phase diagram of the alloy. The surface energy parameter is

$$\Gamma = T_m \gamma V/DL_V mC_\infty(1 - 1/k), \tag{2.10}$$

where T_m is the melting temperature of the pure material, γ is the surface free energy, and L_v is the latent heat per unit volume. Finally, the mean curvature of the interface, H, is given by

$$2H = \nabla \cdot \left[\nabla h(1 + |\nabla h|^2)\right]^{-1/2}. \tag{2.11}$$

3. Linear stability analysis

The basic state for this system takes the form

$$\bar{u} = (1-R)\left[e^{-Bz}\cos(t - Az) - \cos t\right]$$
$$+ R(e^{-z/s} - 1), \tag{3.1a}$$

$$\bar{w} = 0, \tag{3.1b}$$

$$\bar{C} = 1 - e^{-z}, \tag{3.1c}$$

$$\bar{h} = 0, \tag{3.1d}$$

where A and B are constants given in Appendix A. To analyze the response of this state to infinitesimal perturbations, we disturb each of these quantities, and separate the disturbances into normal modes

$$u = \bar{u} + \hat{u}(z, t) e^{i\alpha x} e^{\sigma t} + c.c., \tag{3.2a}$$

$$w = \hat{w}(z, t) e^{i\alpha x} e^{\sigma t} + c.c., \tag{3.2b}$$

$$C = \bar{C} + \hat{C}(z, t) e^{i\alpha x} e^{\sigma t} + c.c., \tag{3.2c}$$

$$h = \hat{h}(t) e^{i\alpha x} e^{\sigma t} + c.c. \tag{3.2d}$$

Here we are seeking time-periodic eigenfunctions, and σ is the Floquet exponent. If the real part of σ is not zero, then the disturbances will experience a net growth or decay over one period. It will turn out that σ is identically zero on the neutral curve in the limit $\epsilon \rightarrow 0$. This means that, in this limit, the response will have the same frequency as the forcing.

By taking the curl of the Navier–Stokes equations twice, and using the continuity equation to simplify the result, we arrive at a fourth-order

disturbance equation for the vertical component of the disturbance velocity. Combining this with the disturbance equation for the solute field we have a sixth-order boundary-value problem. Because the shape of the interface is also undetermined, we require an additional interfacial condition, giving us a total of seven boundary conditions.

In the fluid we have

$$(D^2 + D - \alpha^2 - \Omega\partial_t)\hat{C}$$

$$= \epsilon(i\alpha\bar{u}\hat{C} + e^{-z}\,\hat{w}) + \Omega\sigma\hat{c}, \qquad (3.3a)$$

$$(D^2 - \alpha^2)\big[S(D^2 - \alpha^2) + D - \Omega\partial_t\big]\hat{w}$$

$$= i\alpha\epsilon\big[\bar{u}(D^2 - \alpha^2)\hat{w} - \hat{w}D^2\bar{u}\big]$$

$$+ \Omega\sigma(D^2 - \alpha^2)\hat{w}, \qquad (3.3b)$$

where D indicates $\partial/\partial z$ and ∂_t indicates $\partial/\partial t$.

In the far field, as $z \to \infty$, we have

$$\hat{C}(z, t) \to 0, \qquad (3.4a)$$

$$\hat{w}(z, t) \to 0, \qquad (3.4b)$$

$$D\hat{w}(z, t) \to 0. \qquad (3.4c)$$

The interfacial conditions, transferred to $z = 0$, are

$$M^{-1}\hat{h} = \hat{h}(1 - \alpha^2\Gamma) + \hat{C}, \qquad (3.5a)$$

$$(k - 1)(\hat{C} + \hat{h}) + \Omega\hat{h}_t = D\hat{C} - (1 - \sigma)\hat{h}, \qquad (3.5b)$$

$$\hat{w} = 0, \qquad (3.5c)$$

$$D\hat{w} = i\alpha\hat{h}D\bar{u}. \qquad (3.5d)$$

To proceed further with the analysis, we assume the lateral motion of the crystal is weak so that the parameter ϵ is small, and expand the dependent variables as series in powers of ϵ,

$$\hat{w} = \hat{w}_0 + \epsilon\hat{w}_1 + \ldots, \qquad (3.6a)$$

$$\hat{h} = \hat{h}_0 + \epsilon\hat{h}_1 + \ldots, \qquad (3.6b)$$

$$\hat{C} = \hat{C}_0 + \epsilon\hat{C}_1 + \epsilon^2\hat{C}_2 + \ldots. \qquad (3.6c)$$

We shall seek conditions on the morphological number M such that the system is neutrally stable. To this end, we assume that the real part of

σ is zero, and expand both M^{-1} and the imaginary part of σ in powers of ϵ:

$$M^{-1} = M_0 + \epsilon^2 M_2 + \ldots, \qquad (3.7a)$$

$$\sigma = \epsilon\sigma_1/\Omega + \ldots. \qquad (3.7b)$$

The lower-order terms omitted from these last expansions turn out to be zero, and we have shown explicitly only the terms necessary to resolve the leading-order correction to the neutral-stability curve.

We substitute these expansions into the disturbance equations, set the coefficients of corresponding powers of ϵ to zero, and obtain the following sequence of equations to be solved successively:

$$L_1\hat{C}_0 \equiv (D^2 + D - \alpha^2 - \Omega\partial_t)\hat{C}_0 = 0, \qquad (3.8a)$$

$$L_2\hat{w}_0 \equiv (D^2 - \alpha^2)\big[S(D^2 - \alpha^2) + D - \Omega\partial_t\big]\hat{w}_0$$

$$= 0, \qquad (3.8b)$$

$$L_1\hat{C}_1 = i\alpha\bar{u}\hat{C}_0 + e^{-z}\,\hat{w}_0 + \sigma_1\hat{C}_0, \qquad (3.8c)$$

$$L_2\hat{w}_1 = i\alpha\bar{u}(D^2 - \alpha^2)\hat{w}_0 - i\alpha\hat{w}_0 D^2\bar{u}$$

$$+ \sigma_1(D^2 - \alpha^2)\hat{w}_0, \qquad (3.8d)$$

$$L_1\hat{C}_2 = i\alpha\bar{u}\hat{C}_1 + e^{-z}\,\hat{w}_1 + \sigma_1\hat{C}_1. \qquad (3.8e)$$

The interfacial boundary conditions give (after eliminating h)

$$D\hat{C}_0 = (k + \beta k - 1)\hat{C}_0, \qquad (3.9a)$$

$$\hat{w}_0 = 0, \qquad (3.9b)$$

$$D\hat{w}_0 = i\alpha\beta\hat{C}_0 D\bar{u}, \qquad (3.9c)$$

$$D\hat{C}_1 = (k + \beta k - 1)\hat{C}_1 + \beta\Omega\partial_t\hat{C}_1 + \beta\sigma_1\hat{C}_0, \qquad (3.9d)$$

$$\hat{w}_1 = 0, \qquad (3.9e)$$

$$D\hat{w}_1 = i\alpha\beta\hat{C}_1 D\bar{u}, \qquad (3.9f)$$

$$D\hat{C}_2 = [k + \beta k - 1]\hat{C}_2 + \beta\Omega\partial_t\hat{C}_2 - k\beta^2 M_2\hat{C}_0$$

$$+ \beta\sigma_1\hat{C}_1, \qquad (3.9g)$$

where $\beta = (M_0 + \alpha^2\Gamma - 1)^{-1}$.

Table 1
The parameter values used in the calculations (unless indicated otherwise)

Parameter	Symbol	Value	Units
Kinematic viscosity	ν	2.43×10^{-3}	cm^2/s
Solute diffusivity	D	3.0×10^{-5}	cm^2/s
Liquidus slope	m	-2.33	$K/wt\%$
Melting point	T_m	600.6	K
Surface free energy	γ	42.6	erg/cm^2
Latent heat per unit volume	L_V	2.56×10^9	erg/cm^3
Far field concentration	C_∞	0.01	$wt\%$
Temperature gradient	G	200.0	K/cm
Pulling speed	V	0.01	cm/s
Segregation coefficient	k	0.3	–
Schmidt number	S	81.0	–
Surface energy parameter	Γ	0.6	–

At leading order, the problem reduces to the morphological stability problem in the absence of flow, and the results are equivalent to those found by Mullins and Sekerka [14]:

$$\hat{C}_0 = b_0 e^{-s_0 z}, \tag{3.10a}$$

$$M_0 = 1 - \alpha^2 \Gamma - k(k + s_0 - 1)^{-1}. \tag{3.10b}$$

Here b_0 is an arbitrary constant that does not affect the result of the linear stability analysis, and will be taken to be unity, and s_0 is

$$s_0 = \tfrac{1}{2}\left(1 + \sqrt{1 + 4\alpha^2}\right). \tag{3.11}$$

To illustrate these results, we choose parameter values characteristic of a lead–tin alloy (unless indicated otherwise). These choices are presented in Table 1.

Fig. 2 shows the neutral-stability curve for a lead–tin system in the absence of flow with Γ fixed. If M_0 is above this curve for a given wavenumber, then a disturbance with that wavenumber will decay. Similarly, if M_0 is below this curve for a given wavenumber, then the disturbance will grow. For the interface to be stable for an arbitrary disturbance, M_0 must be above this curve for all α. The wavenumber for the least stable mode is denoted as α_c, and the corresponding morphological number, M_c, is called the critical morphological number, denoting the threshold of instability.

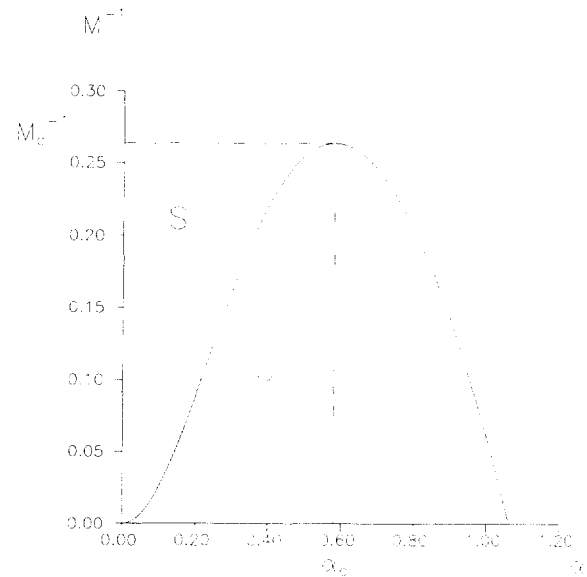Fig. 2. Directional solidification without flow: M^{-1} versus α for $S = 81.0$, $k = 0.3$ and $\Gamma = 0.6$. The region above the curve corresponds to a stable (S) interface, and the region below the curve corresponds to an unstable (U) interface.

Fig. 3 gives $M_c^{-1} \equiv M_{0c}$ and α_c as functions of Γ. If $M_0 < M_{0c}$, then the interface is unstable. For $\Gamma > 1/k$ the interface is always stable; this is
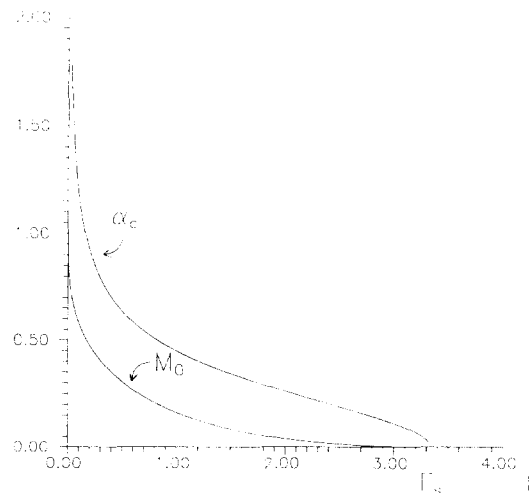

Fig. 3. Directional solidification without flow: The critical value (maximized over wavenumbers) of M_c^{-1} and the critical wavenumber as a function of Γ for $S = 81.0$ and $k = 0.3$. Stable and unstable regions lie above and below the M_c^{-1}-versus-Γ curve, respectively. The absolute stability limit is $\Gamma_s = 1/k$.

known as the absolute stability limit. The critical wavenumber indicates, on a linear theory basis, the width of the cells that form when the interface becomes unstable.

Up to this point we have presented the equations and boundary conditions for the general flow we wish to consider – a combination of an ASP and a CSL. Although these two flows combine linearly to form the basic state, this is not the case in the disturbance equations, where the basic state appears in the coefficients of the equations. However, to the order in ϵ that we are interested in, the two components do not interact, and the general response can be obtained by adding the response to each component determined separately. An explanation for why this is so will be provided in Section 6, but for now we find it convenient to proceed by considering each element of the flow separately.

4. Response to a compressed Stokes layer

For this section, $R = 0$, so $\bar{u}$ will be

$$\bar{u} = e^{-Bz} \cos(t - Az) - \cos t, \tag{4.1}$$

and σ will turn out to be identically zero on the neutral curve.

The solutions to Eqs. (3.8b) through (3.8d) are

$$\hat{w}_0 = a_0(e^{-\alpha z} - e^{-s_1 z}) \, e^{it} - \text{c.c.}, \tag{4.2a}$$

$$\hat{C}_1 = \left(b_1 \, e^{-(s_0 + \bar{r})z} + b_2 \, e^{-(\alpha + 1)z} + b_3 \, e^{-(s_1 + 1)z}\right.$$
$$\left. + b_4 \, e^{-s_0 z} + b_5 \, e^{-s_2 z}\right) e^{it} - \text{c.c.}, \tag{4.2b}$$

$$\hat{w}_1 = a_1 \, e^{-s_3 z} + a_2 \, e^{-(s_1 + \bar{r})z} + a_3 \, e^{-(\alpha + \bar{r})z}$$
$$+ a_4 \, e^{-\alpha z} + a_5 \, e^{-s_1 z} + \text{c.c.} + \text{TDM}. \tag{4.2c}$$

The coefficients and exponents in these expressions are given in Appendix A. The time-dependent modes (TDM) in the solution for $\hat{w}_1$ have been omitted because they do not affect the leading-order correction to the neutral-stability boundary.

At leading order, the flow is forced through the boundary condition (3.5d), leading to a time-periodic response. At $O(\epsilon)$, the disturbance concentration field, $\hat{C}_1$, is also time periodic, but $\hat{w}_1$ consists of both time-dependent and steady parts.
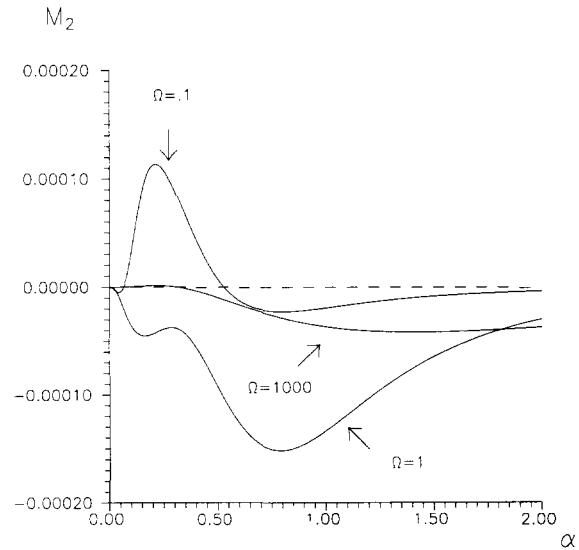

Fig. 4. Directional solidification into CSL: M_2 versus α for $S = 81.0$, $k = 0.3$ and various Ω. M_2 is independent of Γ. When M_2 is above the x-axis, the influence of the flow is destabilizing, and when M_2 is below the x-axis, the influence of the flow is stabilizing. As $\Omega \to \infty$, $M_2 \to 0$, and as $\Omega \to 0$, M_2 approaches a steady state. Note that for $\Omega = 1$ the flow is stabilizing for all wavenumbers.

Only the steady parts of $\hat{w}_1$ affect the neutral-stability results, however. M_1 is determined to be zero at this order.

The correction to the neutral-stability curve, M_2, is determined by applying a solvability condition to the $O(\epsilon^2)$ solute equation. This condition is necessary because the steady forcing terms at this order reproduce, upon separation of variables, the eigenfunction of the leading-order problem. The leading-order problem is homogeneous, and has nontrivial solutions, so the inhomogeneous problem found at this order will have solutions only if the inhomogeneity satisfies

$$M_2 = \frac{1}{\beta^2 k} \int e^{-(s_0 - 1)z} \, f(z) \, dz, \tag{4.3}$$

where $f(z)$ is the forcing term in the $O(\epsilon^2)$ solute equation.

A plot of $M_2(\alpha)$ for various nondimensional forcing frequencies is shown in Fig. 4. It turns out that M_2 is independent of Γ, the surface energy parameter. Note that the actual neutral-stability curve is given by the sum $M_0 + \epsilon^2 M_2$, where
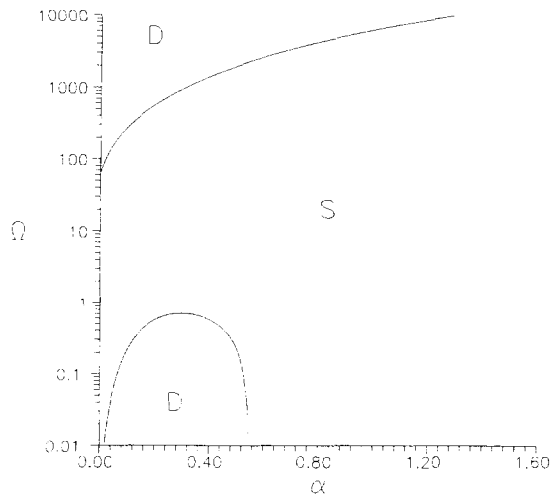
Fig. 5. Directional solidification into CSL: Regions of the α–Ω plane where the flow stabilizes (S) or destabilizes (D) the interface relative to the case without flow. $S = 81.0$ and $k = 0.3$; result is independent of Γ.

$\epsilon = U/V$ is assumed small. When $M_2 > 0$, the flow destabilizes the interface, and when $M_2 < 0$, the flow stabilizes. As $\Omega \to \infty$, the Stokes boundary-layer thickness, $\delta_{SL} = (2\nu/\omega)^{1/2}$, approaches zero, and the flow has a vanishingly small effect on stability. As $\Omega \to 0$, the boundary-layer thickness approaches that for the ASP, $\delta_{ASP} = \nu/D$, and the flow approaches a quasisteady limit, with M_2 approaching a finite value. The quasisteady limit of M_2 is qualitatively similar to the result for the ASP (see section 5 and Fig. 7).

Fig. 4 reveals that for many values of Ω the effect of the flow on morphological stability can be either stabilizing or destabilizing, depending on the wavenumber of the disturbance. However, there is a range of Ω values for which the flow stabilizes the interface against disturbances of arbitrary wavenumber. This *window of stabilization* is seen more clearly in Fig. 5, where we indicate the regions of the α–Ω plane where the flow stabilizes ($M_2 < 0$) and destabilizes ($M_2 > 0$) the interface compared to the no-flow case.

For the lead–tin system, the range of Ω for which the flow is necessarily stabilizing is approximately 1–50. This corresponds to a dimensional oscillation frequency of $f \approx 0.5$–25.0 cycles per second for a pulling speed of 100 μm/s.

When Ω lies outside of the window of stabilization, the actual influence the flow will have depends on the location of the critical wavenumber for the onset of instability in the case without flow. If this critical wavenumber lies in one of the regions of the α–Ω plane where the flow is destabilizing, then the flow will make the interface less stable. Since $\epsilon^2 M_2$ is assumed to be much smaller than that of M_0, we can assert the converse as well; for if the peak of the curve in Fig. 2 is slightly stabilized when some point away from the peak is slightly destabilized, the net effect will be to stabilize the interface. The possible exceptions to the this last claim would occur if the two points in question were close together. This would happen when the values of α_c and Ω indicate a location close to one of the boundaries in Fig. 5.

As an example of how the various parameters conspire to influence the stability of the interface, consider two cases: one in which the flow can either stabilize or destabilize depending on α_c, and one in which the flow always stabilizes the interface. Notice from Fig. 3 that the location of α_c is determined by Γ only given S and k. Using
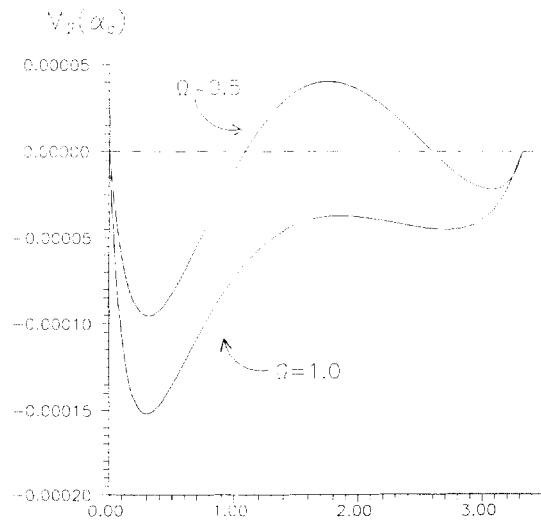

Fig. 6. Directional solidification into CSL: Plot of $M_2(\alpha_c)$ versus Γ for $S = 81.0$, $k = 0.3$ and $\Omega = \{0.5, 1.0\}$. Note that when $\Omega = 1$ the flow has stabilized the interface for all Γ, but when $\Omega = 0.5$ the flow is destabilizing for a range of Γ.

this relationship between Γ and α_c, in Fig. 6 we plot $M_2(\Gamma)$ for the two scenarios just described. These curves are the corrections to the curve shown in Fig. 3, where we plot $M_0(\Gamma)$. The lower curve corresponds to a value of $\Omega = 1$, which places it inside of the window of stabilization in Fig. 5; M_2 is negative for all values of Γ along this curve, indicating the flow will stabilize the system for all values of Γ as expected. The upper curve corresponds to a value of $\Omega = 0.5$, which means there is a range of critical wavenumbers that will place it in the region of destabilization in the lower portion of Fig. 5. Along this curve, M_2 starts out negative, then becomes positive before returning to negative values as Γ is increased. The values of Γ for which M_2 is positive correspond to situations where the CSL will destabilize the interface relative to the no-flow case, i.e. $\alpha_c(\Gamma)$ lies in the region of destabilization.

All of our results to this point have been for a specific alloy. We find that the window of stabilization persists for a wide range of material parameters (segregation coefficient and Schmidt number). There is a tendency for the window to rise with increasing Schmidt number, and to narrow with increasing segregation coefficient.

5. Response to an asymptotic suction profile

For this section $R = 1$, so $\bar{u}$ will be

$$\bar{u} = 1 - e^{-z/S}, \tag{5.1}$$

and σ_1 will turn out to be nonzero, indicating the presence of travelling waves.

The solutions to Eqs. (3.8b) through (3.8d) are

$$\hat{w}_0 = a_0(e^{-\alpha z} - e^{-s_1 z}) \tag{5.2a}$$

$$\hat{C}_1 = b_1 \, e^{-(s_0 + 1/S)z} + b_2 \, e^{-(\alpha + 1)z} + b_3 \, e^{-(s_1 + 1)z}$$
$$+ b_4 z \, e^{-s_0 z} \tag{5.2b}$$

$$\hat{w}_1 = a_1 \, e^{-s_1 z} + a_2 \, e^{-(s_1 + 1/S)z} + a_3 \, e^{-(\alpha + 1/S)z}$$
$$+ a_4 \, e^{-\alpha z} + a_5 z \, e^{-s_1 z} \tag{5.2c}$$

The coefficients and exponents in these expressions are given in Appendix B. Note that although similar notation is used, these are not
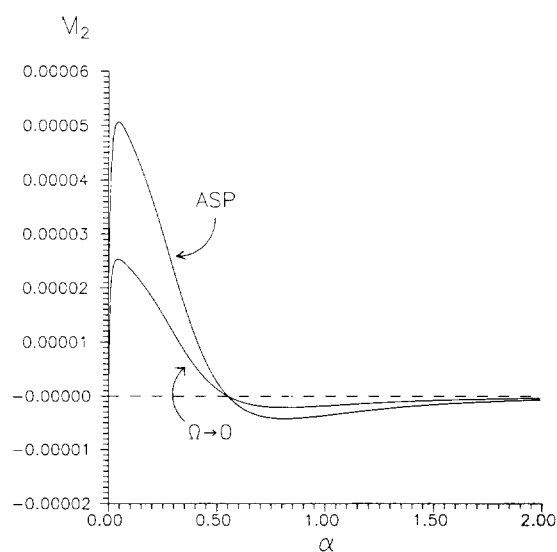

Fig. 7. Directional solidification into ASP: M_2 versus α for $S = 81.0$, $k = 0.3$. M_2 is independent of Γ. When $M_2 > 0$, the influence of the flow is destabilizing, and when $M_2 < 0$, the influence of the flow is stabilizing. The quasisteady limit of the CSL case is shown for comparison.

necessarily the same coefficients and exponents as in the previous section.

In Fig. 7 we plot M_2 versus α for the ASP and the quasisteady limit of the CSL. The ASP result, as with M_2 for the CSL, is independent of Γ, but there are no other parameters to vary for the ASP. Qualitatively, the result for the ASP agrees with Fig. 5 in the article by Hobbs and Metzener [10], except for long-waves. Their paper indicates that $M_2 \sim \alpha^{-2}$ as $\alpha \to 0$. We find that M_2 is $O(1)$ in this limit. Personal communication with Hobbs has revealed that some minor algebraic errors are responsible for these discrepancies. The focus of their paper is on a long-wave analysis designed to resolve the nonuniformity in the expansion of M^{-1} as $\alpha \to 0$. Despite the fact that M_2 is $O(1)$ and not $O(\alpha^{-2})$ as $\alpha \to 0$, there is still a nonuniformity in the expansion since $M_0 \to 0$ as $\alpha \to 0$. It would appear, however, that this nonuniformity does not seriously impair the validity of the expansion, since our results agree qualitatively (a quantitative comparison has not been made) with the uniform results they present in later sections of their paper.

6. Combined response

For this section, $0 < R < 1$, and $\bar{u}$ is a linear combination of the basic states for the CSL and ASP, taking the form

$$\bar{u} = (1 - R)\left[e^{-Bz} \cos(t - Az) - \cos t\right]$$
$$+ R(e^{-z/S} - 1). \tag{6.1}$$

Notice that the CSL portion of the flow is time periodic and the ASP portion is steady. The steady basic-state concentration profile does not depend on the flow.

One's understanding of this system can be greatly enhanced by simply recognizing which terms are steady and which are time periodic. In general, a time-periodic forcing function will not have a net effect on the long-term behavior of the system, unless it is coupled with another time-periodic forcing to produce "steady-streaming".

Using the results for the CSL and ASP, it turns out that we can simply add solutions to find the morphological response to the combined flow. When we seek asymptotic solutions in the limit $\epsilon \to 0$, the basic state appears only in the inhomogeneous terms of disturbance equations and boundary conditions. When the products in these inhomogeneous terms are expanded, the inhomogeneities are seen to contain terms that correspond to those encountered when the CSL and ASP were considered individually, plus some additional time-periodic terms that do not affect the leading-order morphological-stability results. Thus, there is no coupling of the two solutions at this order.

So, for this section

$$M_2 = (R - 1)M_{2SL} + RM_{2ASP}, \tag{6.2}$$

where M_{2SL} is the M_2 of Section 4, and M_{2ASP} is the M_2 of Section 5.

For the combined flow, we investigate the influence of the parameters R and Ω with the segregation coefficient and Schmidt number fixed at the values for a lead–tin alloy. We do so by looking at a diagram analogous to that shown in Fig. 5, where we mapped out regions of the $\alpha-\Omega$ plane where the flow stabilized and destabilized the interface with respect to the no-flow results.
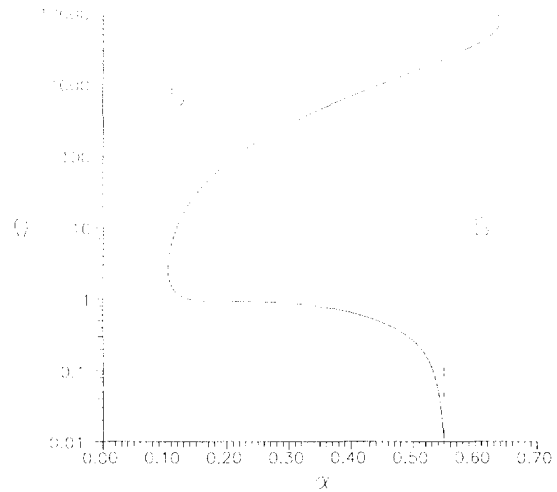

Fig. 8. Directional solidification into combined flow: Regions of the $\alpha-\Omega$ plane where the flow stabilizes (S) or destabilizes (D) the interface relative to the case without flow. $S = 81.0$, $k = 0.3$, and $R = 0.5$. The dashed vertical line corresponds to the case $R = 1$ (ASP only), with the region to the left of the line destabilizing, and the region to the right stabilizing.

Fig. 5 is the result for the CSL only ($R = 0$). For the ASP ($R = 1$) our results are independent of Ω, and this diagram consists of a single vertical line emanating from $\alpha \approx 0.55$. Disturbances with wavenumbers larger (smaller) than this will be stabilized (destabilized). For intermediate values of R the curves shown in Fig. 5 evolve into the simple picture just described as R is increased from zero to one. In Fig. 8 we show the result for $R = 0.5$. Notice that there is no window of stabilization.

7. Mechanisms affecting stability

In this section we shall provide a physical interpretation of our results in terms of mechanisms that promote or inhibit morphological instability. We begin with the no-flow case, which serves as the leading-order effect for both flows, followed by the CSL and, finally, a few comments on the ASP.

The fate of the interface is controlled by the temperature and concentration fields, along with surface tension on the interface. In the model we

are using, the temperature field is fixed and lin-
ear, with a positive gradient, i.e. the temperature
increases into the melt. This has a stabilizing
effect on the interface; for if cells start to form,
advancing portions of the interface will meet with
higher temperatures than portions lagging be-
hind, and will be melted back.

The local melting temperature is determined
by the Gibbs–Thomson equation:

$$T = T_M - 2T_M H\gamma/L_V + mC, \qquad (7.1)$$

where T is the temperature of the interface
(melting temperature), T_M is the melting temper-
ature of the pure material, H is the mean curva-
ture of the interface, γ is the surface free energy,
L_V is the latent heat per unit volume, and m is
the liquidus slope in the phase diagram. The
second term in the right-hand side of this equa-

tion accounts for the Gibbs–Thomson effect, or
capillary undercooling, which dictates that the
local melting temperature is decreased by an
amount proportional to the local curvature. Pro-
truding sections of the interface will tend to be
melted back as a result; thus, surface energy
stabilizes the interface. The third term accounts
for constitutional undercooling, adjusting the
melting temperature by an amount proportional
to the local solute concentration.

It is the mechanism of constitutional under-
cooling that drives the instability. To understand
this, we analyze the concentration linearized
about the interface:

$$C(x, 0 + h', t) \sim \overline{C}(0) + h'(x, t)\,\overline{C}_z(0)$$
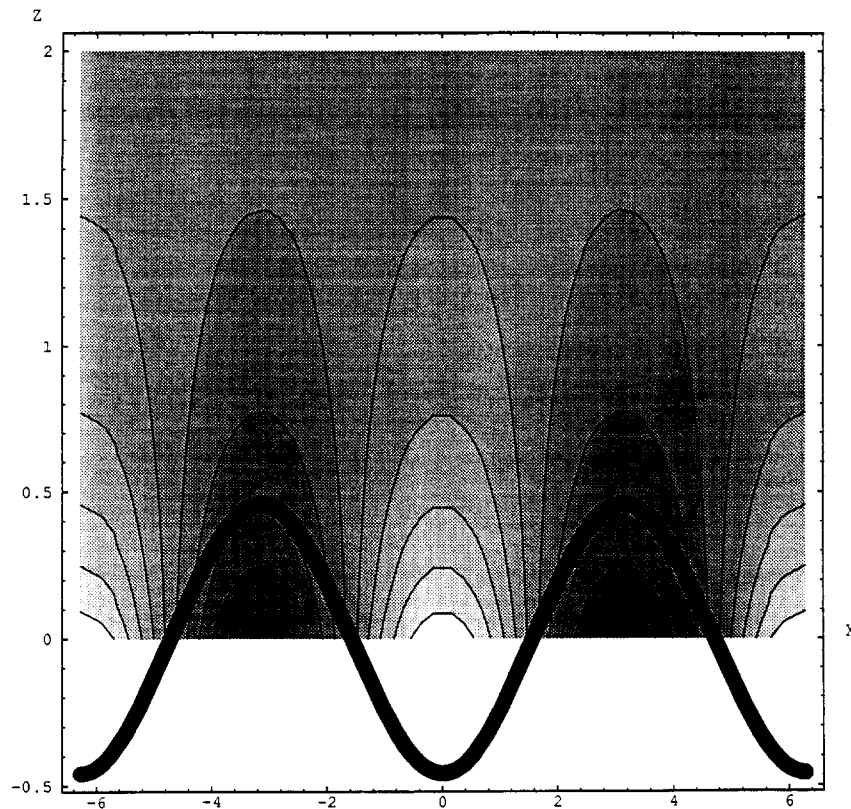$$+ C'(x, 0, t), \qquad (7.2)$$

Fig. 9. Directional solidification without flow: The interfacial disturbance superposed (not to scale) on the disturbance concentra-
tion field (rescaled to agree in sign with the dimensional C) when flow is absent. Notice that the higher concentrations (dark
regions) are near the peaks of the interfacial disturbance, lowering the local melting temperature. This has a stabilizing influence
on the interface.

where the primed quantities are the small pertur-
bations to the basic state. The first term on the
right-hand side is independent of x and t, and
contributes to the basic state. The next term is
the source of the instability; for advancing por-
tions of the solid will encounter lower solute
concentrations as a result of the negative gradi-
ent, $\bar{C}_z(0)$, of the basic-state concentration field.
This results in lower melting temperatures, and
promotes continued growth. The last term is sta-
bilizing because the disturbance to the concentra-
tion field raises the concentration in the neigh-
borhood of a peak in the interface disturbance,
resulting in a higher melting temperature. This
last effect is illustrated in Fig. 9, where we super-
pose the interface shape on the disturbance so-
lute field for a disturbance composed of a single

Fourier mode. It is exclusively through this means
that flow affects the linear stability of the inter-
face – surface energy and interface shape have
no direct effect.

There is nothing in our model that allows the
interface to react directly to hydrodynamic forces;
the solidified material is considered non-com-
pliant. Also, recall that the temperature field is
fixed in this model. That being the case, the only
effect that the flow has on stability is to alter the
distribution of solute. We have already noted that
such effects are absent at leading order. For the
CSL, there are also no steady effects at $O(\epsilon)$
because the concentration field at this order is
time periodic and has zero mean. At $O(\epsilon^2)$ there
are both steady and time-periodic forcing terms,
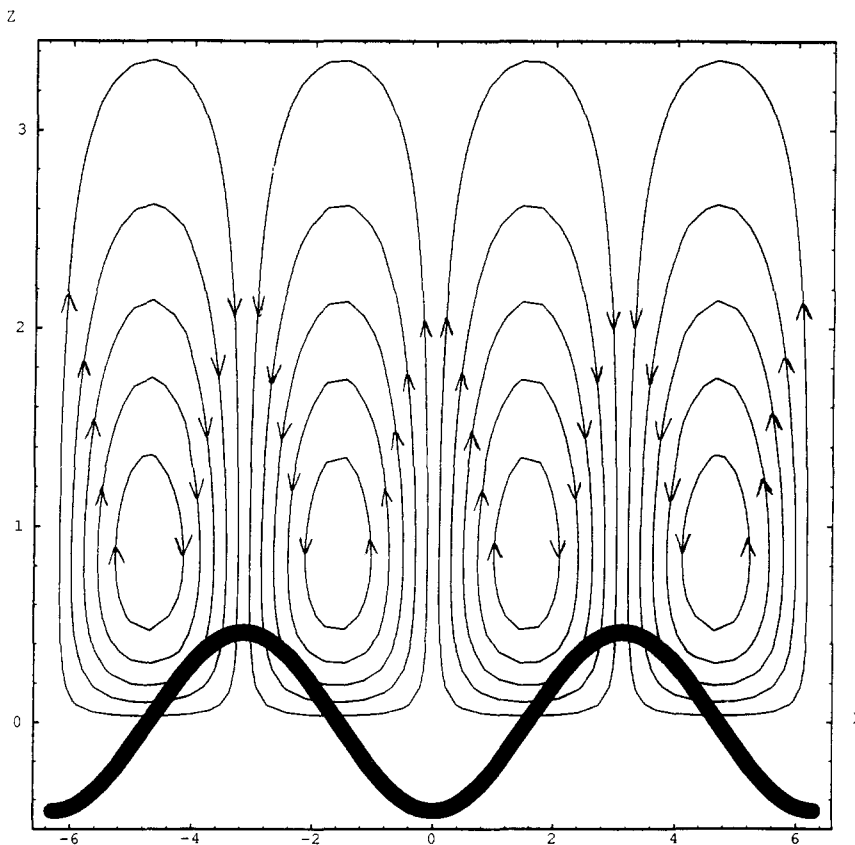with the steady terms giving rise to a steady

Fig. 10. Directional solidification into CSL: The steady streamlines for the flow disturbance impinge on the peaks of the interfacial
disturbance for the lead–tin system when $\Omega = 1.0$. This dilutes the local solute concentration, raising the local melting
temperature. This has a destabilizing influence on the interface.

contribution to the concentration field. Once again, stability is affected through the mechanism of constitutional undercooling; when the concentration of solute is increased over the peaks of a disturbance, the disturbance is stabilized, and when this concentration is decreased, the disturbance is destabilized. This lateral redistribution of solute is determined by the convective fluxes that force the system. Eq. (3.8e), reproduced below, reveals that two types of forcing terms act on the system at this order:

$$L_1 \hat{C}_2 = e^{-z} \, \hat{w}_1 + i \alpha \bar{u} \hat{C}_1. \tag{7.3}$$

First, there is the convection of the base concentration field by the disturbance flow field, and second, there is the convection of the disturbance concentration field by the base flow.

Recall that only steady changes in the concentration field affect stability. In Fig. 10 we plot the steady streamlines for the disturbance velocity field and the leading-order interfacial disturbance for a single Fourier mode. Notice that the streamlines are impinging on the peaks of the disturbance. This means that material that is less solute-laden is being swept toward the peaks from the far-field, lowering the local concentration, which has a destabilizing effect. For other parameter values or disturbance wavenumbers, the streamlines can be made to impinge on the valleys instead, but the streamlines always have the
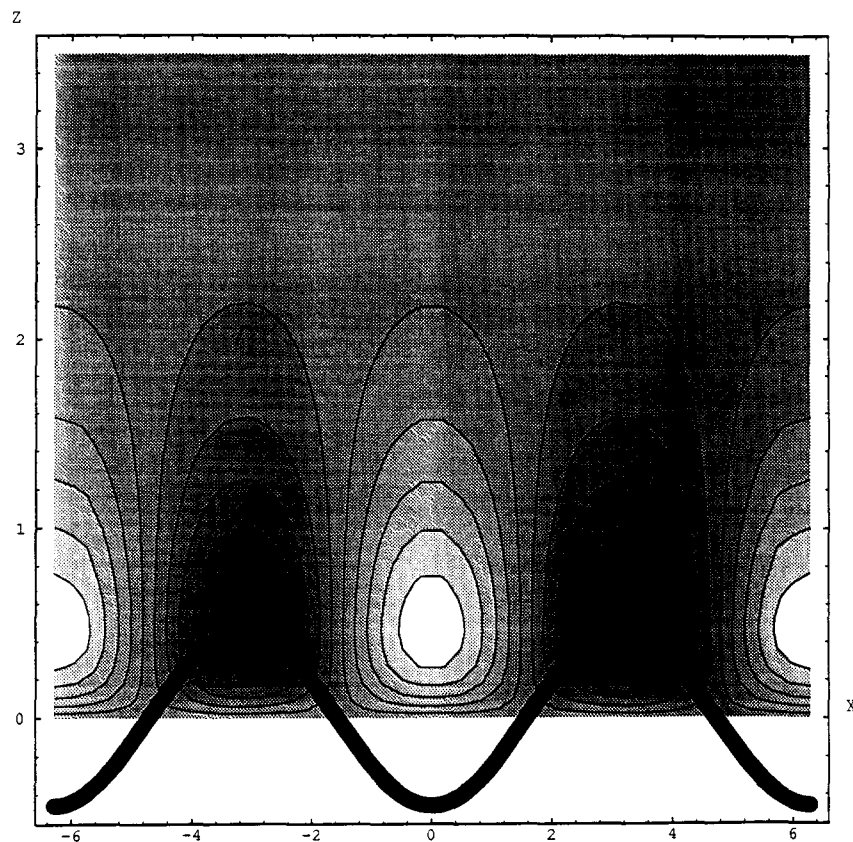

Fig. 11. Directional solidification into CSL: The flux of solute ($i \alpha \bar{u} \hat{C}_1$ of Eq. (7.3)) produced by the interaction of the steady flow field disturbance and the base concentration field (rescaled to agree in sign with the dimensional C) for the lead–tin system when $\Omega = 1.0$. The sinks of solute (lighter regions) are over the valleys in the interfacial disturbance, lowering the local melting temperature. This has a destabilizing influence on the interface.

same period as the interface disturbance and are exactly in or out of phase with it. In Fig. 11 we plot the solute flux that results from the interaction of these streamlines with the basic-state concentration field. Notice that the sinks of solute flux are over the peaks in the interface disturbance.

The streamlines for the base flow are simply lines parallel to the flat interface, which do nothing to transport the base concentration, but interact with the time-periodic correction to the concentration field to produce a steady flux of solute. In Fig. 12 we plot this flux field and the disturbed interface, as before. Notice that there is a source

of solute flux above each peak in the interface disturbance. This stabilizes the interface.

In general these two types of fluxes may compete or cooperate depending on material parameters and disturbance wavenumber. In the case for which we generate these illustrative plots, they compete, and the second, stabilizing, effect wins. This is in agreement with the results presented in Section 4, since these plots are for an Ω lying within the window of stabilization.

We have just demonstrated that the CSL can enhance interfacial stability by the lateral redistribution of solute. Because the instability is driven by the negative vertical concentration gra-
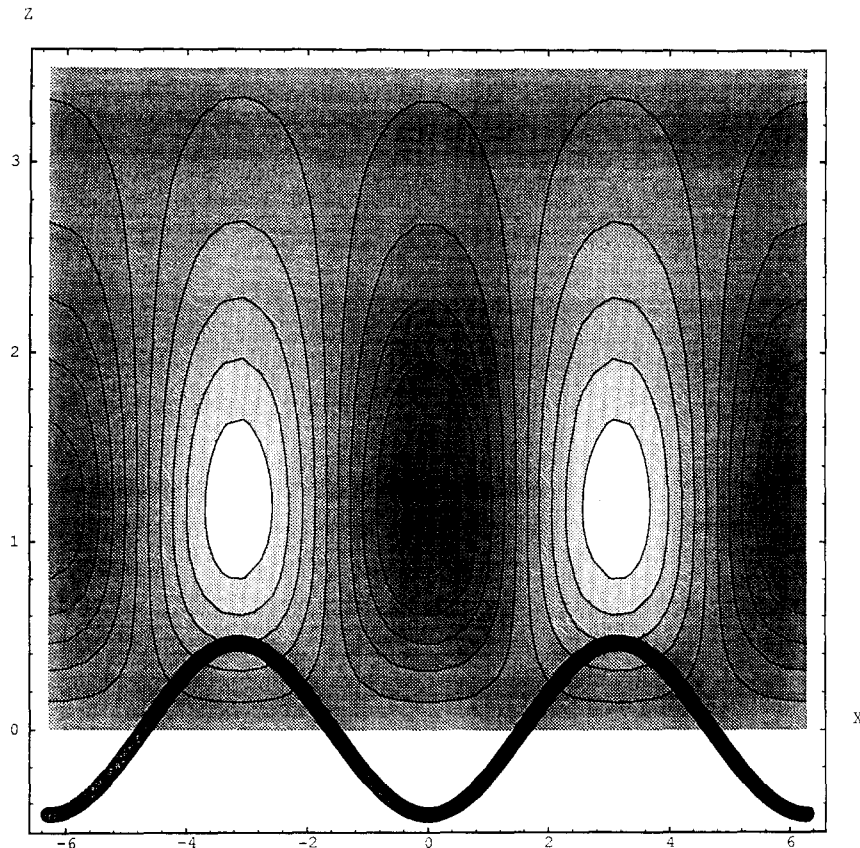

Fig. 12. Directional solidification into CSL: The steady flux of solute ($e^{-z}\hat{w}_1$ of Eq. (7.3)) produced by the interaction of the base flow field and the concentration field disturbance (rescaled to agree in sign with the dimensional C) for the lead–tin system when $\Omega = 1.0$. The sinks of solute (lighter regions) are over the peaks in the interfacial disturbance, lowering the local melting temperature. This has a stabilizing influence on the interface. The magnitude of this effect is greater than the one shown in the previous figure.

dient of the basic state, one might think that the key to stabilizing the interface would lie in smoothing this gradient. If one computes the average vertical concentration gradient, one finds that there is no contribution from linear theory. By retaining higher-order terms one arrives at the following equation for the average solute concentration by integrating over one cycle in time and one wavelength in x, and simplifying the result using the continuity equation:

$$\overline{C}_{zz} + \overline{C}_z = \overline{C'w'_z}. \tag{7.4}$$

Here the overline indicates average over time and space, and the primed quantities are the eigenfunctions determined by linear theory. Solving this equation with the averaged boundary conditions ($C \to 0$ at $z = 0$ and as $z \to \infty$) reveals that the flow actually steepens the concentration gradient in some cases where, according to linear theory, the flow stabilizes the interface.

With the ASP the situation is similar, but now the solute fluxes responsible for shaping the concentration field are steady only when viewed in a reference frame that moves with the $O(\epsilon)$ wave speed, σ_1. As a result, cells should tilt when the interface become unstable.

8. Conclusions

The linear stability analysis has shown that by fixing the frequency of horizontal oscillations of a crystal during its formation one can decrease the range of pulling speeds for which the interface becomes unstable to two-dimensional disturbances. This stabilization is achieved for a finite range of frequencies which we refer to as a window of stabilization. This result is in contrast to the result of Merchant and Davis [13] in their study of an imposed time-periodic stagnation-point flow, where they find that stabilization occurs for a range of low frequencies, including zero. We find that this window of stabilization closes as we increase the segregation coefficient, and rises as we increase the Schmidt number.

When the interface remains unstable in the presence of a CSL, microstructure is significantly affected. Corrugations are formed in the pattern of nonuniformities that normally consists of stripes perpendicular to the mean interface position, and the length scale of the surface morphology is adjusted.

To gain further control over the systems response, one might combine oscillatory motion with a steady translation. In experimental or practical situations, such flows can be approximated by combining an oscillatory and steady crystal rotation. In the limit we have considered – a weak forcing of the flow – we have shown that the individual responses to these two types of flow can be superposed to determine the combined response. We find that the window of stabilization is destroyed by the presence of the steady motion.

In general, the flow affects the stability of the interface by producing periodic changes in the concentration field that have the same spatial scale as the dominant mode of the interface disturbance. These adjustments to the concentration then promote or inhibit instability through the mechanism of constitutional undercooling.

For a practical application of these ideas it would be necessary to understand the effect of a strongly forced flow; for the change produced by what we assumed was a small forcing, will, of course, be small. This can be approached by considering the problem in the limit of large Schmidt number, or by attacking the problem numerically. As we noted earlier, Forth and Wheeler [8] have done this for the ASP. Their results are similar to the results presented here and in Hobbs and Metzener [10] for the small velocity-ratio limit. The numerical results of Forth and Wheeler also indicate that the trends shown for the small velocity-ratio limit continue for larger velocity ratios. It remains to be seen if this is true for the Stokes-layer problem.

A more serious impediment to the practical use of these flows is that they affect only disturbances with wave vectors parallel to them. So even if we dramatically stabilize the two-dimensional system, we do nothing to stabilize the three-dimensional system. Kelly and Hu [11] have shown that the onset of Rayleigh–Bénard convection can be delayed by imposing a nonplanar

oscillation onto the system, which extends the stabilization to three-dimensional disturbances. Such a scheme to stabilize the present system seems promising.

Acknowledgements

Appendix A

The constants in Eq. (3.1) are

$$A = \sqrt{\frac{-1 + \sqrt{1 + 16S^2\Omega^2}}{8S^2}}, \qquad (A.1a)$$

$$B = \frac{1 + \sqrt{1 + \frac{1}{2}\left(-1 + \sqrt{1 + 16S^2\Omega^2}\right)}}{2S}, \qquad (A.1b)$$

and we define

$$r = B + iA, \qquad (A.2a)$$

$$\bar{r} = B - iA. \qquad (A.2b)$$

The exponents in Eq. (3.10) and Eqs. (4.2a) through (4.2c) are

$$s_0 = \left(1 + \sqrt{1 + 4\alpha^2}\right)/2, \qquad (A.3a)$$

$$s_1 = \left(1 + \sqrt{1 + 4S^2\alpha^2 + 4iS\Omega}\right)/2S, \qquad (A.3b)$$

$$s_2 = \left(1 + \sqrt{1 + 4\alpha^2 + 4i\Omega}\right)/2, \qquad (A.3c)$$

$$s_3 = \left(1 + \sqrt{1 + 4S^2\alpha^2}\right)/2S. \qquad (A.3d)$$

The coefficients in Eqs. (4.2a) through (4.2c) are

$$a_0 = -ir\alpha\beta/2(s_1 - \alpha), \qquad (A.4a)$$

$$a_1 = (j_1\alpha - j_2)/(\alpha - s_3), \qquad (A.4b)$$

$$a_2 = \frac{(ia_0\alpha/2)\left(\alpha^2 - s_1^2 + \bar{r}^2\right)}{\left[(s_1 + \bar{r})^2 - \alpha^2\right]\left[S(s_1 + \bar{r})^2 - S\alpha^2 - s_1 - \bar{r}\right]}, \qquad (A.4c)$$

$$a_3 = \frac{-i\alpha a_0\bar{r}^2/2}{\left[(\alpha + \bar{r})^2 - \alpha^2\right]\left[S(\alpha + \bar{r})^2 - S\alpha^2 - \alpha - \bar{r}\right]}, \qquad (A.4d)$$

$$a_4 = (j_2 - j_1 s_3)/(\alpha - s_3), \qquad (A.4e)$$

$$a_5 = a_0\alpha/2\Omega, \qquad (A.4f)$$

$$b_1 = \frac{i\alpha/2}{r(r + 2s_0 - 1) - i\Omega}, \qquad (A.4g)$$

$$b_2 = a_0/(\alpha - i\Omega), \qquad (A.4h)$$

$$b_3 = -a_0 S/\left[S(s_1 - i\Omega) + s_1 + i\Omega\right], \qquad (A.4i)$$

$$b_4 = \alpha/2\Omega, \qquad (A.4j)$$

$$b_5 = \left[i\Omega\beta b_4 + b_2(1 + \alpha - i\Omega\beta - s_0)\right. \\ + b_3(1 + i\Omega\beta + s_1 - s_0) + b_1(i\Omega\beta + r)\right] \\ \times (s_0 - 1 - i\Omega\beta)^{-1}, \qquad (A.4k)$$

where

$$j_1 = -\tfrac{1}{2}(a_2 + a_3 + a_5 + \text{c.c.}), \qquad (A.5a)$$

$$j_2 = -\tfrac{1}{2}\{(s_1 + \bar{r})a_2 + (\alpha + \bar{r})a_3 + s_1 a_5 + \text{c.c.} \\ -\tfrac{1}{2}i\alpha\beta\left[\bar{r}(b_1 + b_2 + b_3 + b_4 + b_5) + \text{c.c.}\right]\} \qquad (A.5b)$$

The correction to the neutral stability curve, M_2, is

$$M_2 = \frac{1}{\beta^2 k}\left[\frac{a_1}{s_0 \mp s_3} + \frac{a_2}{\bar{r} + s_0 + s_1} + \frac{a_3}{\alpha + \bar{r} + s_0}\right. \\ + \frac{a_4}{\alpha + s_0} + \frac{a_5}{s_0 + s_1} - \tfrac{1}{2}i\alpha\left(\frac{b_1}{2s_0 + r - 1}\right. \\ + \frac{b_2}{\alpha + s_0} + \frac{b_3}{s_0 + s_1} + \frac{b_4}{2s_0 - 1} + \frac{b_5}{s_0 + s_2 - 1} \\ - \frac{b_1}{2B + 2s_0 - 1} - \frac{b_2}{\alpha + \bar{r} + s_0} - \frac{b_3}{\bar{r} + s_0 + s_1} \\ \left.\left. - \frac{\bar{b}_4}{\bar{r} + 2s_0 - 1} - \frac{\bar{b}_5}{\bar{r} + s_0}\right) + \text{c.c.}\right]. \qquad (A.6)$$

Appendix B

The exponents in Eqs. (5.2a) through (5.2c) are

$$s_0 = \left(1 + \sqrt{1 + 4\alpha^2}\right)/2, \tag{B.1a}$$

$$s_1 = \left(1 + \sqrt{1 + 4S^2\alpha^2}\right)/2S. \tag{B.1b}$$

The coefficients in Eqs. (5.2a) through (5.2c) are

$$a_0 = i\alpha\beta/S(s_1 - \alpha), \tag{B.2a}$$

$$a_1 = ia_0/(1 + 2S\alpha), \tag{B.2b}$$

$$a_2 = -ia_0\alpha(1 - s_1 S)/2s_1(1 + 3s_1 S), \tag{B.2c}$$

$$a_3 = \frac{-ia_0(\alpha^2 - s_1^2)(i\sigma_1 - \alpha)}{-4s_1^3 S + 3s_1^2 + 4\alpha^2 s_1 S - \alpha^2}, \tag{B.2d}$$

$$a_4 = [(a_1 + a_2)(s_1 S - 1) - i\alpha\beta(b_1 + b_2 + b_3) - (\alpha a_1 - a_3 + a_2 s_1)S]/(\alpha - s_1)S, \tag{B.2e}$$

$$a_5 = [(a_1 + a_2)(1 - \alpha S) + i\alpha\beta(b_1 + b_2 + b_3) + (\alpha a_1 - a_3 + a_2 s_1)S]/(\alpha - s_1)S, \tag{B.2f}$$

$$b_1 = -i\alpha S/(2s_0 + 1/S - 1), \tag{B.2g}$$

$$b_2 = a_0/\alpha, \tag{B.2h}$$

$$b_3 = -a_0 S/s_1(S + 1), \tag{B.2i}$$

$$b_4 = (\sigma_1 + i\alpha)/(1 - 2s_0). \tag{B.2j}$$

The wavespeed σ_1 is

$$\sigma_1 = \left\{-i\alpha + (1 - 2s_0)[b_0/S + (\alpha + 1 - s_0)b_1 + (s_1 + 1 - s_0)b_2]\right\}(1 - \beta + 2\beta s_0)^{-1} \tag{B.3}$$

and the correction to the inverse morphological number is

$$M_2 = \frac{1}{\beta^2 k}\left[\frac{a_1}{\alpha + s_0 + S^{-1}} + \frac{a_2}{\alpha + s_1 + S^{-1}}\right.$$
$$+ \frac{a_3}{s_0 + s_1^2} + \frac{a_4}{\alpha + s_0} + \frac{a_5}{s_0 + s_1}$$

$$+ (\sigma_1 + i\alpha)\left(\frac{b_1}{2s_0 - 1 + S^{-1}} + \frac{b_2}{\alpha + s_0}\right.$$
$$\left. + \frac{b_3}{s_0 + s_1} + \frac{b_4}{2s_0 - 1^2}\right)$$
$$- i\alpha\left(\frac{b_1}{2s_0 - 1 + 2S^{-1}} + \frac{b_2}{\alpha + s_0 + S^{-1}}\right.$$
$$\left. + \frac{b_3}{s_0 + s_1 + S^{-1}} + \frac{b_4}{2s_0 - 1 + S^{-1^2}}\right)$$
$$\left. + \beta\sigma_1(b_1 + b_2 + b_3)\right]. \tag{B.4}$$

References

[1] S.R. Coriell and G.B. McFadden, in: Handbook of Crystal Growth, Vol. 1B, Ed. D.T.J. Hurle (North-Holland, Amsterdam, 1993) p. 785.

[2] S.R. Coriell, G.B. McFadden, R.F. Boisvert and R.F. Sekerka, J. Crystal Growth 69 (1984) 15.

[3] S.R. Coriell, G.B. McFadden and R.F. Sekerka, Ann. Rev. Mater. Sci. 15 (1985) 119.

[4] S.H. Davis, J. Fluid Mech. 212 (1990) 241.

[5] S.H. Davis, in: Interactive Dynamics of Convection and Solidification, Eds. S.H. Davis, H.E. Huppert, U. Müller and M.G. Worster (Kluwer, Dordrecht, 1992) p. 31.

[6] S.H. Davis, in: Handbook of Crystal Growth, Vol. 1B, Ed. D.T.J. Hurle (North-Holland, Amsterdam, 1993) p. 859.

[7] R.T. Delves, J. Crystal Growth 8 (1971) 3.

[8] S.A. Forth and A.A. Wheeler, J. Fluid Mech. 202 (1989) 339.

[9] M.E. Glicksman, S.R. Coriell and G.B. McFadden, Ann. Rev. Fluid Mech. 18 (1986) 307.

[10] A.K. Hobbs and P. Metzener, J. Crystal Growth 112 (1991) 539.

[11] R.E. Kelly and H.-C. Hu, J. Fluid Mech. 249 (1993) 373.

[12] J.S. Langer, Rev. Mod. Phys. 52 (1980) 1.

[13] G.J. Merchant and S.H. Davis, J. Crystal Growth 96 (1989) 737.

[14] W.W. Mullins and R.F. Sekerka, J. Appl. Phys. 35 (1964) 444.